The Concurrent Complementary Operators Method for FDTD Mesh Truncation

Omar M. Ramahi, *Member, IEEE*

***Abstract*— The complementary operators were developed for the purpose of truncating the computational domain of finite-difference time-domain (FDTD) open-region simulations. In the original implementation of the complementary operators method, two independent simulations were performed. The solutions from these two simulations were then averaged to obtain a solution devoid of first-order reflections. In this paper, the complementary operators are implemented in a concurrent fashion. This new implementation, referred to as the concurrent complementary operators method (C-COM), requires only one simulation, thus reducing the operation count by approximately one half. The implementation for two-dimensional (2-D) space is outlined first with emphasis on reducing reflections from corner regions; then the extension to three dimensions is developed. Numerical results are provided in addition to an analysis of the source of error that arises from this new implementation.**

***Index Terms*— FDTD methods.**

I. Introduction

THE complementary operators method (COM) was originally introduced as a mesh truncation technique for open-region finite-difference time-domain (FDTD) simulations [1], [2]. The basic premise of the COM is the cancellation of the first-order reflection that arises when the computational domain is terminated with a single-equation boundary operator or absorbing boundary condition (ABC). This cancellation is made possible by averaging two independent solutions to the problem. These two solutions are obtained by imposing boundary operators that are complementary to each other. Two operators are considered to be complementary if their reflection coefficients are equal in magnitude but are 180° out of phase. Therefore, the two solutions that are generated from applying each of the two operators separately, when averaged, result in a solution that does not contain any of the first-order reflections. The primary strength of the COM is that the cancellation of the first-order reflections takes place for any field independent of the wave number, which implies that effective suppression of the reflections occur whether the fields are composed of evanescent or purely traveling waves.

The COM requires two independent solutions of the problem, which lead to doubling the total operation count in comparison to the traditional implementation of ABC's. Despite this, however, the COM was found to be highly effective and efficient in comparison to other mesh truncation techniques [2]-[4]. This is primarily due to the fact that the COM allows the terminal boundaries to be brought very close to the radiating structure. Despite the COM effectiveness, nevertheless, it would still be even more desirable to avoid two independent simulations, since the overhead requirement of the simulation is then reduced by one half, and further allows for effective modeling of nonlinear media [3]. In a recent letter, a new implementation of COM was presented [5]. In this implementation, instead of applying each of the operators in a separate simulation, the complementary operators were applied concurrently. This new implementation is referred to as the concurrent complementary operators method (C-COM). In this paper, we review the theory of complementary operators as was originally implemented in the COM method. Next, we discuss the implementation and performance of the concurrent implementation of the COM in two-dimensional (2-D) space, followed by an extension to three-dimensional (3-D) space. Finally, we analyze the source of spurious reflections that arise when using the C-COM method.

Manuscript received August 19, 1997; revised June 5, 1998.

The author is with the Compaq Computer Corporation, PKO3-1/R1, Maynard, MA 01754 USA.

Publisher Item Identifier S 0018-926X(98)07495-X.

II. Complementary Operators Method

The concept underlying the COM method is the application of two independent boundary operators given by

$$B_N^- U = \partial_x \prod_{i=1}^{N} \left(\partial_x + \frac{\cos\phi}{c}\,\partial_t + \alpha_i \right) U = 0 \tag{1}$$

$$B_N^+ U = \partial_t \prod_{i=1}^{N} \left(\partial_x + \frac{\cos\phi}{c}\,\partial_t + \alpha_i \right) U = 0 \tag{2}$$

where U is the unknown field on which the boundary condition is applied and c is the speed of light [3]. The parameter α_i ensures the stability of the simulation and has been shown empirically to depend on the cell size and the dimensionality of the problem, and is typically $\alpha_i = 0.02/\Delta s$ and $\alpha_i = 0.1/\Delta s$ for 2-D and 3-D space, respectively. The angle ϕ can be optimized to minimize reflection in a specific propagation direction. In a general application, however, where no advanced knowledge of propagation is assumed, ϕ is set to zero.

For a time-harmonic plane wave, the reflection coefficients for B_N^- and B_N^- are given respectively by

$$R[B_N^-] = \prod_{i=1}^{N} \frac{-jk_x + jk\cos\phi + \alpha_i}{jk_x + jk\cos\phi + \alpha_i} \tag{3}$$

$$R[B_N^+] = (-1) \prod_{i=1}^{N} \frac{-jk_x + jk\cos\phi + \alpha_i}{jk_x + jk\cos\phi + \alpha_i}. \tag{4}$$

Both of these operators result in reflection coefficients that are equal in magnitude; that is $|R[B_N^-]| = |R[B_N^+]|$. The

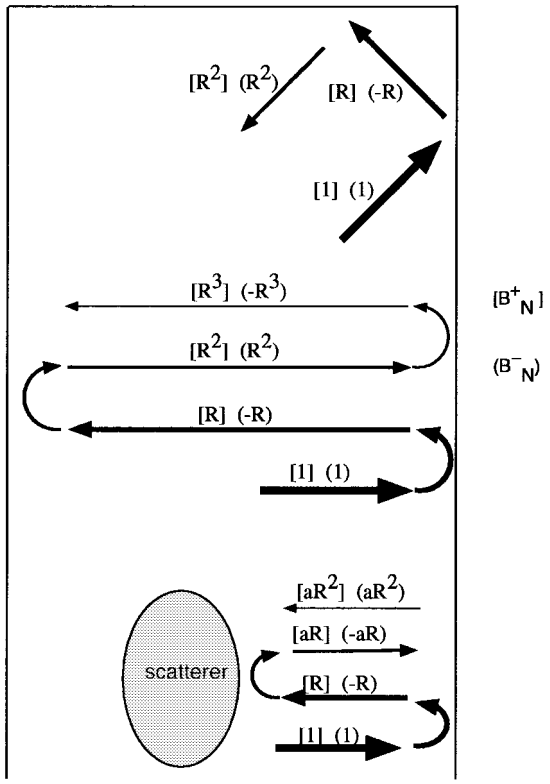

Fig. 1. Multiple reflections due to terminal boundaries, corner regions, and the scatterer (for simplicity, the scatterer is assumed to reflect the field by a factor a).

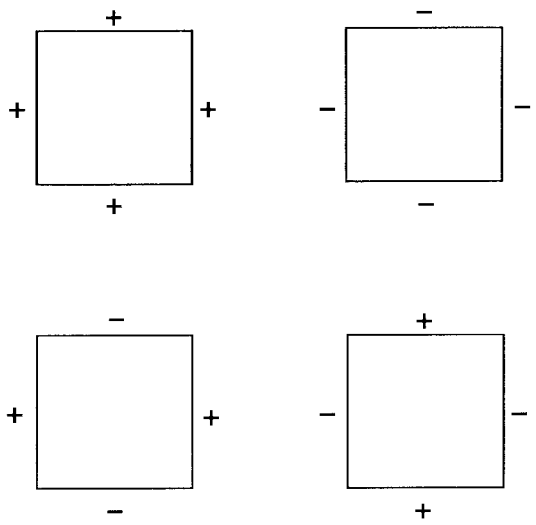

Fig. 2. The four different permutations of boundary operators needed to annihilate corner reflections for 2-D space.

TABLE I
CORNER REGION REFLECTIONS

	1st reflection (R1)	2nd reflection (R2)
solution #1	R	R^2
solution #2	$-R$	R^2
solution #3	R	$-R^2$
solution #4	$-R$	$-R^2$

averaging of the two solutions obtained from applying each of the two operators separately, gives a solution containing only second-order reflections, including those that arise from corner regions. An illustration of the cancellation that takes place when these two operators are applied separately to two independent simulations is given in Fig. 1. In this figure, we show the reflections that take place when the incident wave interacts with the side boundaries and corner regions. In Fig. 1, we assume the original radiating pulse has a magnitude of one and denote the reflections due to B_N^- by brackets and the reflections due to B_N^+ by parentheses.

Clearly visible from Fig. 1 is that second-order reflections arising from the corner regions are not annihilated when the two solutions are averaged. These reflections, although second-order in nature, can be a significant source of error since the fields impinge at the corners at highly oblique angles, which cause the second-order reflection to remain substantial in comparison to second-order reflections coming from the sides. For instance, when using COM4 [employing (1) and (2) with $N = 3$], a wave incident at the corner at an angle of 70° comes back into the domain with approximately 1% reflection.

To cancel corner region reflections in 2-D space, four independent simulations (instead of two) would be needed. For each simulation, one needs to impose a unique combination of B_N^- and B_N^+ over the four sides of the outer boundary as shown in Fig. 2, where for brevity, we use $+$ to denote B_N^+ and $-$ to denote B_N^-.

Further illustration is shown in Table I. the magnitudes of the first- and second-order reflections due to the upper-right corner (assuming an incident pulse of unity magnitude) for each of the four needed solutions. Notice that the average of all the values in the second column eliminates the corner reflections.

In the original implementation of the COM, the focus was on the annihilation of first-order reflections and, thus, only two independent simulations were considered. The four solution scheme was avoided because it was believed to lead to an excessive operation count for practical problems requiring large space and a large number of time steps. The concurrent implementation of COM is intended to achieve the two objectives: 1) implement the complementary operators within one single simulation and 2) allow the annihilation of corner region reflections.

III. CONCURRENT COMPLEMENTARY OPERATORS METHOD IN TWO-DIMENSIONAL SPACE

The concurrent implementation of the COM involves the application of complementary operators at a distance from the terminal boundary (into the computational domain) such that the first-order reflections are canceled right before they reenter the computational domain. The implementation entails dividing the FDTD computational space into two regions—a boundary layer and an interior region. The interior region includes the scattering object and any localized sources.

First, we illustrate the application of the C-COM to reduce reflections from side boundaries only. To this end, we assign two storage (memory) locations to each nodal field in the

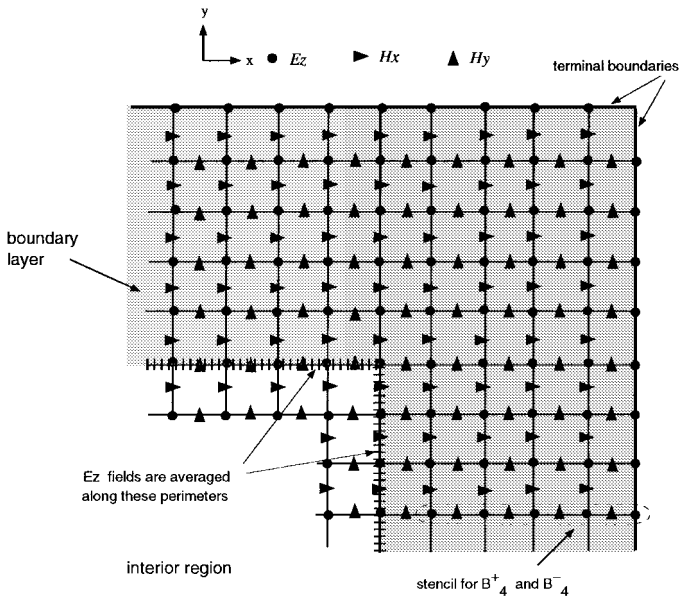

Fig. 3. Boundary layer showing the field locations and the averaging interface. Also shown is the stencil needed to discretize B_4^+ and B_4^-.

boundary layer. (The following discussion focuses only on the treatment for the TM polarization case; the TE polarization is fully analogous.) We denote the two storage locations assigned to E_z as $E_z^{(1)}$ and $E_z^{(2)}$. Similar assignment is made for H_x and H_y, giving $H_x^{(1)}$, $H_x^{(2)}$ and $H_y^{(1)}$, $H_y^{(2)}$, respectively.

Within the interior region, each of the field components is assigned a single storage location, as in typical FDTD implementation. Within the boundary layer, $E_z^{(1)}$ and $E_z^{(2)}$ are updated independently using their associated H fields. Next, we apply the two boundary operators (1) and (2) to $E_z^{(1)}$ and $E_z^{(2)}$, respectively. Notice that each set of fields in the boundary layer is updated independently of the other set. This amounts to having two independent simulations in the boundary layer.

The next step is to connect the solutions in the two regions. This is performed by averaging the two values obtained for each field at the interface lying between the interior region and the boundary layer. The exact location of this interface defines the width of the boundary layer. This width directly impacts the additional memory overhead that will be required in comparison to standard ABC implementation. The width of the boundary layer is required to be at least the width (size) of the stencil which is essential for the discretization of the ABC in (1) or (2). Fig. 3 highlights the corner segment of an FDTD mesh where, for illustration, we show a five-cell wide boundary layer for the TM polarization case.

The above steps required for the implementation of the C-COM are summarized as follows.

1) E_z, H_x, and H_y are updated in the interior region according to standard FDTD equations.
2) On the mesh terminal boundary, apply B_N^- on $E_z^{(1)}$ and B_N^+ on $E_z^{(2)}$.
3) Within the boundary layer, $E_z^{(1)}$ is updated from $H_x^{(1)}$ and $H_y^{(1)}$ and $E_z^{(2)}$ is updated from $H_x^{(2)}$ and $H_y^{(2)}$. Both sets are updated using standard FDTD equations.
4) $E_z^{(1)}$ and $E_z^{(2)}$ are averaged along the interface connecting the two regions (see Fig. 3). The new values of $E_z^{(1)}$ and $E_z^{(2)}$ along the interface are given the value of the average $(E_z^{(1)} + E_z^{(2)})/2$.
5) Advance time by one-half time step.
6) Update H_x and H_y in the interior region. At the interface, H_x and H_y in the interior region will use $(E_z^{(1)} + E_z^{(2)})/2$ as calculated in (4).
7) In the boundary layer, $H_x^{(1)}$ and $H_y^{(1)}$ are updated using $E_z^{(1)}$ and $H_x^{(2)}$ and $H_y^{(2)}$ are updated using $E_z^{(2)}$.

We mention here that if the averaging is carried out at an interface placed within the stencil of the ABC [(1) or (2)], then the solution becomes unstable as will be explained in the section on analysis.

The procedure outlined above annihilates reflections arising from side boundaries. To extend the annihilation to corner reflections, four storage locations need to be assigned to each field in the boundary layer to account for second-order reflections. For each field set, i.e., $(E_z^{(i)}, H_x^{(i)}, H_y^{(i)}, i = 1, 2, 3, 4)$, one of the ABC combinations shown in Fig. 2 is applied. Then an identical averaging procedure to the one outlined above is performed, with the exception of having four field values to update in the boundary layer and four field values to average at the interface.

In a manner consistent with the nomenclature used for the COM method [3], the C-COM employing a fourth-order operator [$N = 3$ in (1) and (2)] will be denoted as C-COM4. For this, the width of the stencil is five cells inclusive of the boundary node. Furthermore, we use two additional parameters to fully identify the methodology used in terms of doubling or quadrupling the fields in the boundary layer and its width. When the fields are doubled in the boundary region resulting in the cancellation of side reflections only, we refer to the method as C-COM4 (2, W), where W indicates the width of the boundary layer. Similarly, when the fields are quadrupled in the boundary region, annihilating corner reflections, we refer to the method as C-COM4 (4, W).

To demonstrate the performance of the C-COM4, we first consider an experiment chosen such that the reflections due to the sides and corners of the computational domain are clearly distinguished from the incident (reflection-free) pulse. We consider a space of size 400 $\Delta s\times$ 400 Δs. The excitation is a line current source (impressed current) located at (100 Δs, 100 Δs). We consider a uniform mesh in the x- and y-directions, with a space step of $\Delta s = 0.015$ m and time step of $\Delta t = 0.9\Delta t_c$ seconds, where Δt_c is the Courant limit.

The observation point is at (50 Δs, 50 Δs). The pulse is chosen narrow enough to isolate the reflections as stated earlier. The excitation waveform is a compact pulse given by the convolution $h(t)*h(t)$ where $h(t)$ is defined over the time interval $0 \le t \le \tau$ and is given by

$$h(t) = \pi 10^4 (15\sin(\omega_1 t) - 12\sin(\omega_2 t) + 3\sin(\omega_3 t)) \quad (5)$$

where $\tau = 10^{-9}$ and $\omega_i = 2\pi i/\tau$, $i = 1, 2, 3$.

Fig. 4 shows a segment of the computational domain emphasizing the primary reflections that contribute to the signal level at the observation point. Notice that the sides and

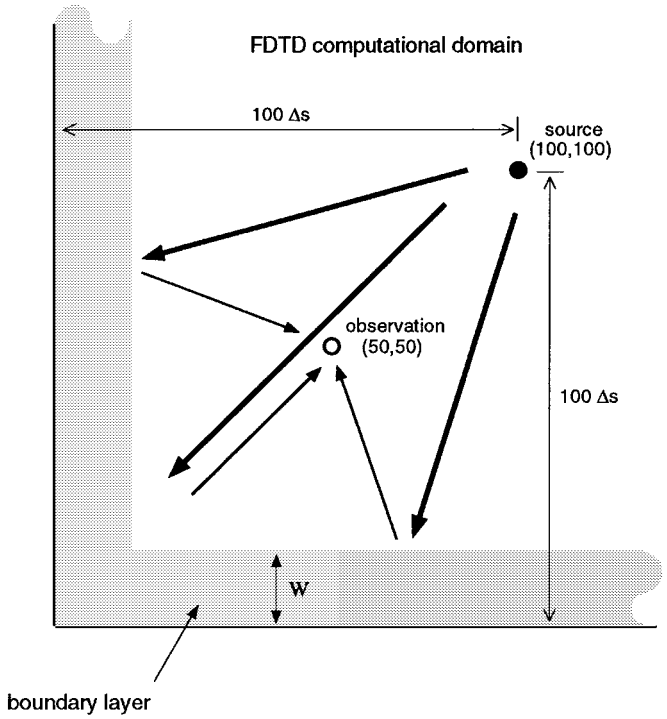

Fig. 4. Part of the 400 Δs × 400 Δs computational domain highlighting dominant reflections arising from side and corner regions.

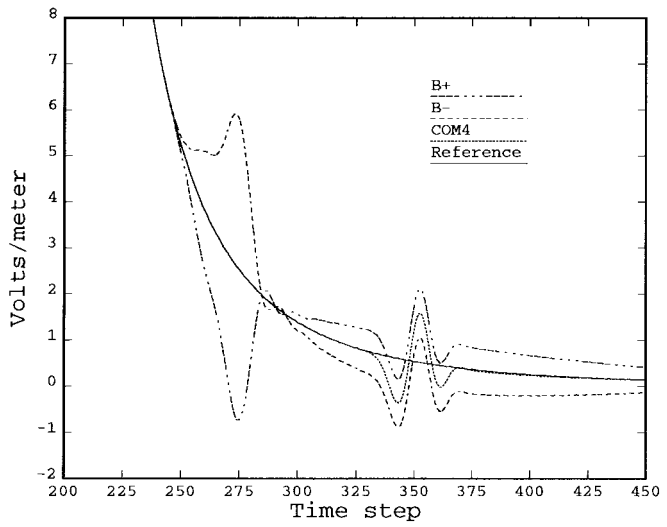

Fig. 5. E_z field at observation point (50 Δs, 50 Δs) showing side and corner reflections.

corners that are not shown contribute reflections that will not be present in the solution window that was intentionally considered. In Fig. 5, we show the solutions obtained using COM4, B_4^-, and B_4^+ (B_4^- and B_4^+ are referred to in Fig. 5 as B^- and B^+, respectively). A comparison is made with the reference solution. For this and the following experiments, the reference solution is a reflection-free solution obtained in a domain large enough such that the boundary reflections do not appear in the solution time window.

In Fig. 5, we note that the reflection due to the sides is clearly visible as it is the first to arrive at the observation point. Also shown in the figure is the reflection due to

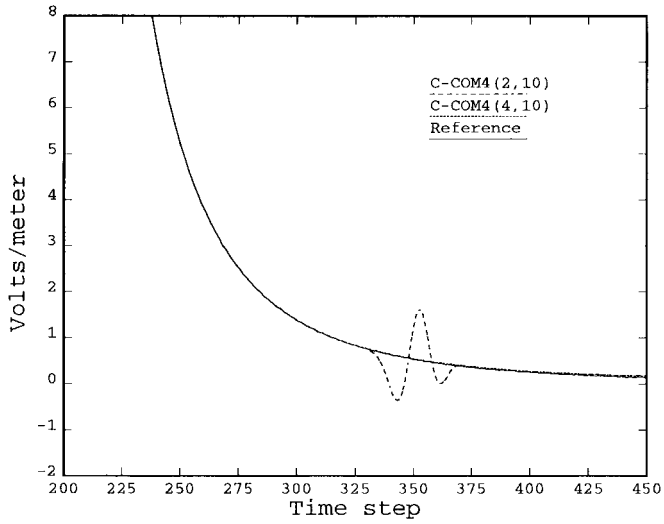

Fig. 6. E_z field at observation point (50 Δs, 50 Δs) showing the C-COM4 (4, W) annihilation of side and corner reflections.

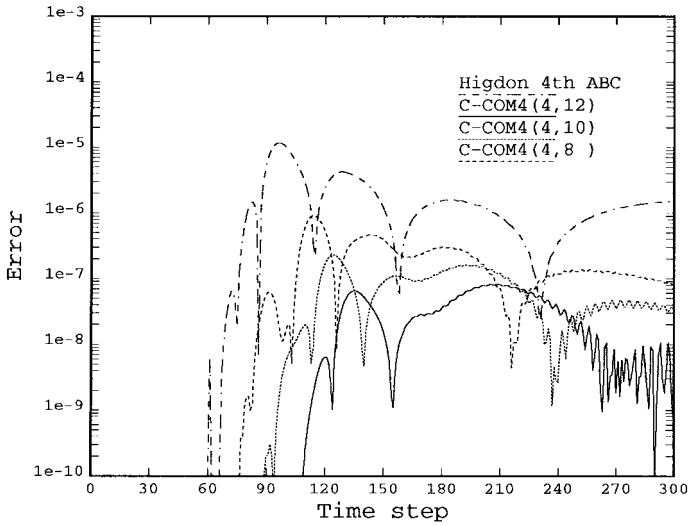

Fig. 7. Effect of varying the width of the boundary layer on accuracy.

the corner region when the COM is applied. (The corner reflection corresponds to the second glitch in the signal.) Fig. 6 shows how the C-COM4 (4, 10) can be quite successful in annihilating side and corner reflections, whereas, C-COM4 (2, 10) cannot reduce the corner reflection. For a perspective on the error levels seen in Figs. 5 and 6, we note that the maximum amplitude of the solution waveform is 7.22×10^4 and it occurs at $t = 141\Delta t$.

A second experiment is provided to show the level of improvement achieved when considering a more practical scenario where the terminal boundary is close to the source of radiation. Here, we choose a space of size 21 $\Delta s\times$ 21 Δs. The boundary layer will then be added to this space as will be shown below. A line current source positioned at (11 Δs, 11 Δs), and an observation point is chosen close to the source at (16 Δs, 16 Δs) . The excitation waveform, space and time steps are as before. In Fig. 7, we show the effect of varying the width of the boundary layer, from 8–12 cells. Comparison is made with Higdon's fourth-order ABC. Here, the results are

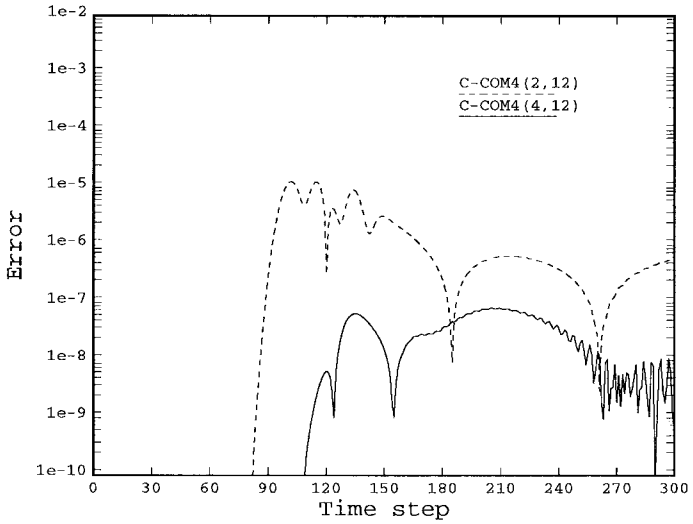

Fig. 8. Error from using C-COM4 (2, 12) and C-COM4 (4, 12).

presented in terms of the normalized absolute error defined a

$$Error(t) = \frac{|y(t) - y^{ref}(t)|}{\max[|y^{ref}(t)|]} \tag{6}$$

where $y(t)$ is the solution that corresponds to the C-COM4 or Higdon fourth ABC solutions and $y^{ref}(t)$ is the reference solution.

Fig. 8 shows the improvement achieved when using C-COM4 (4, 12) over COM4(2, 12) for the same size geometry. Notice that C-COM4(2, 12) gives a solution very comparable to COM4 as would be expected. What is important to note from these results is that corner reflections comprise a significant portion of the total reflected field. This is in accordance with the predictions made earlier about the relatively high reflection coefficients arising from waves impinging on the corner regions at highly oblique angles.

Before concluding this section, we present a third numerical experiment to show the performance of the C-COM method in treating waves traveling at near grazing incidence. For this purpose, we consider reflection from one side of the computational domain. The size of the FDTD domain is 1800 $\Delta s\times$ 218 Δs. A line source is positioned at (300 Δs, 18 Δs) and three observation points, OP1, OP2, and OP3 are situated at (450 Δs, 18 Δs), (560 Δs, 18 Δs), and at (1300 Δs, 18 Δs), respectively, as shown in Fig. 9. The corresponding angles of incidence (measured with respect to the normal) at the terminal boundary for OP1, OP2, and OP3 are 76.5°, 82°, and 88°, respectively. The FDTD source and space parameters are chosen as before.

Notice that the domain was chosen such that the only artificial reflections that appear in the solution over the time duration of interest arrive from the nearest terminal boundary, which is the only one shown in Fig. 9.

In this test, we study the behavior of a 16-layer C-COM. This layer makes the distance between the source or observation points and the layer 2 Δs. Fig. 10(a)–(c) shows the pulse as it arrives at the three observation points. Here, we show a comparison between the solution obtained using C-COM4 (2, 16) and a 16-layer perfectly matched layer (PML)

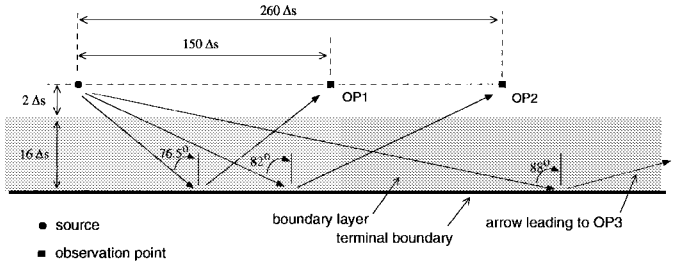

Fig. 9. Reflection of waves traveling at near grazing incidence.

[6] employing a quadratic conductivity profile and a normal incidence theoretical reflection of 10^{-5}. In accordance with [6], the PML solution is denoted as PML (16, 3, 10^{-5}). Comparison is also made to the reference solution, which is devoid of any terminal boundary reflections.

This numerical experiment demonstrates the effectiveness of the C-COM method in predicting solutions with high degree of accuracy even when the solution is composed of waves traveling at near-grazing incidence to the terminal boundary. We also see that for OP3, the angle of incidence at the boundary is approximately 88° and for this, both the PML and the C-COM show higher deviation than what was obtained when the observation points had lower angles of incidence, which would be intuitively expected. However, clearly visible from Fig. 10(c) is that the C-COM4 solution strongly resembles the shape of the reference solution, whereas the PML deviation is observed to be in magnitude as well as in form.

Further scrutiny of the PML and the C-COM4 solutions is made possible by looking at their respective frequency-domain responses. Fig. 11 shows the frequency response of the PML and C-COM solutions for OP3 (88° angle of incidence). The frequency response is obtained by performing Fourier transformation using 2048 points. (In Fig. 11, the abscissa corresponds to the normalized frequency which assumes a unity time step.) Fig. 11 shows a maximum error in the C-COM 4 (2, 16) solution of approximately 3 dB, which occurs at the frequency corresponding to the maximum amplitude in the reference solution (the numerically exact solution). The PML solution, on the other hand, is seen to deviate markedly, especially in predicting the maximum amplitude frequency.

IV. Concurrent Complementary Operators Method in 3-D Space

The extension of the C-COM implementation to 3-D space is performed in an entirely analogous fashion to the implementation in 2-D space. To suppress reflections arising from side boundaries (single-reflection), two storage locations need to be reserved for each field in the boundary layer. The annihilation of corner reflections, however, and unlike the 2-D space case, would require a total of eight storage locations for each field in the boundary layer. This is because the cancellation of corner reflections requires the imposition of eight possible unique permutations of (1) and (2) at the boundaries (2^M, where M is the number of sides forming a single corner). Notice that in the computational space, there are two types

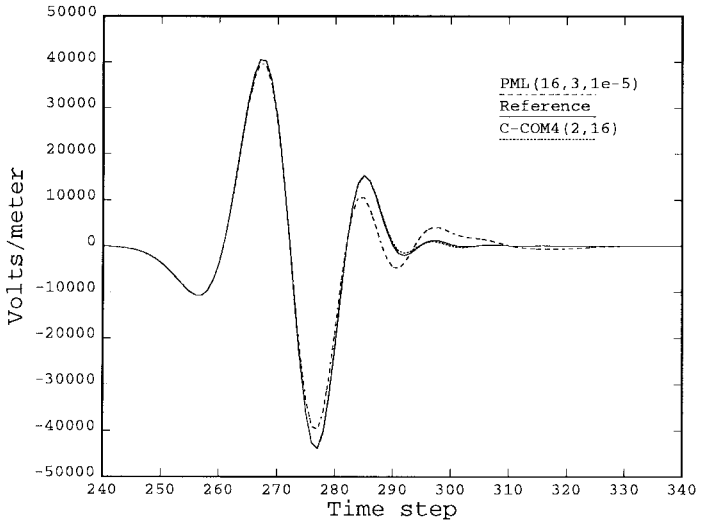

(a)

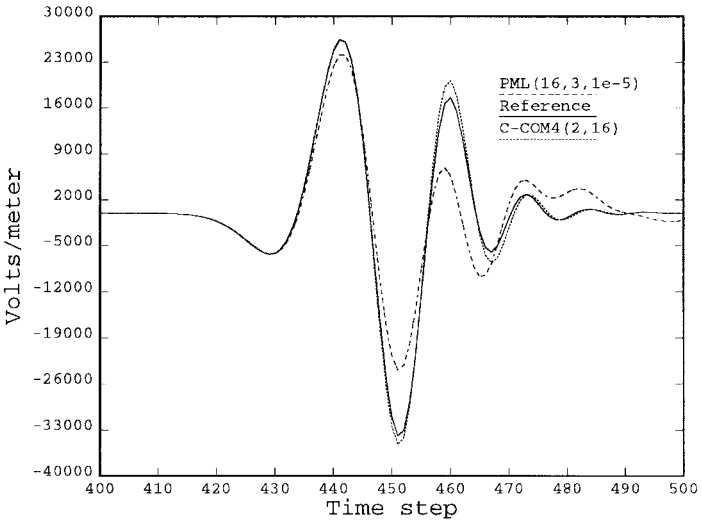

(b)

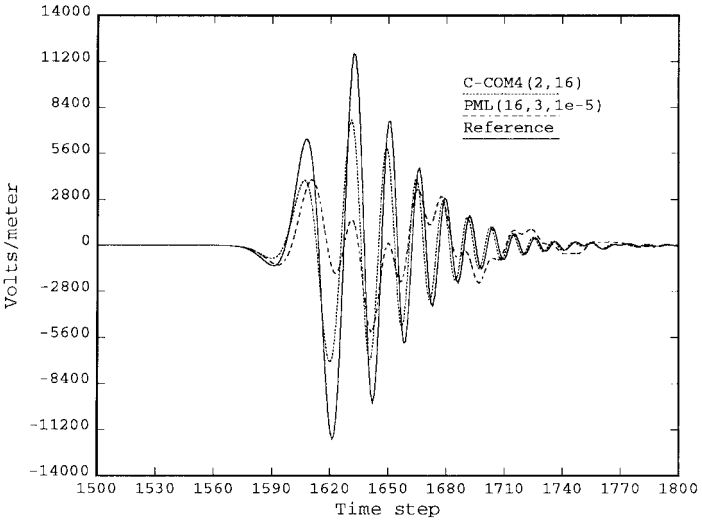

(c)

Fig. 10. (a) Solution at OP1 corresponding to 76.5° angle of incidence at the terminal boundary. (b) Solution at OP2 corresponding to 82° angle of incidence at the terminal boundary. (c) Solution at OP3 corresponding to 88° angle of incidence at the terminal boundary.

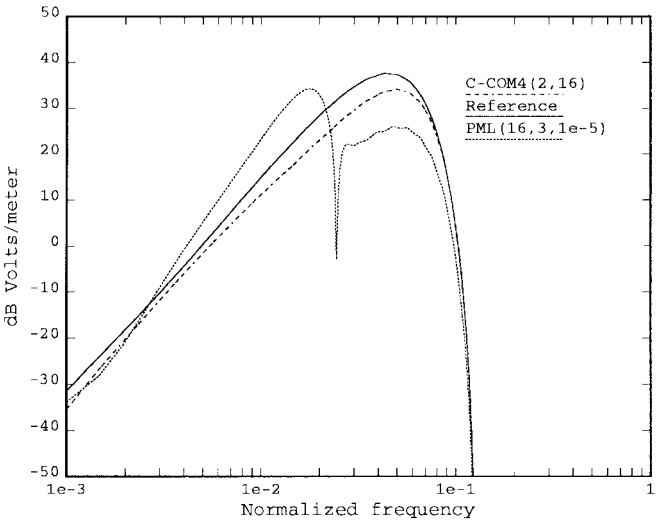

Fig. 11. Frequency domain response at OP3 corresponding to 88° angle of incidence at the terminal boundary.

of corners. The first type is a corner formed by two planes; the second is the one formed by three planes. It can easily be demonstrated that the cancellation of secondary reflections arising from either of the two types of corners would require eight storage locations.

Consistent with the nomenclature for the 2-D space, we denote C-COM4 (2,W) and C-COM4 (8,W) as corresponding to the implementation where the fields in the boundary layer are either doubled or increased eight-fold, respectively.

To test the effectiveness of C-COM4 in space, we consider the experiment in which a z-polarized Herzian dipole is located in the center of the computational space having uniform space steps in the x, y, and z directions of $\Delta s = 0.001\ m$. Here we consider a space of size 21 $\Delta s\times$ 21 $\Delta s\times$ 21 Δs inclusive of the boundary layer to make the point that the observation point can be positioned within the boundary layer.

The time step is $\Delta t = 0.9\Delta t_c$ seconds. The excitation waveform is a Gaussian pulse modulating a sinusoidal signal

$$f(t) = \cos(\omega t)\, e^{-((T-T_o)/w)^2} \tag{7}$$

where $T_0 = 160\Delta t$, $w = 40\Delta t$, and $\omega = 30\pi 10^{10}$.

The results are presented in terms of the absolute normalized error [as in (6)] in the E_z field at an observation point eight cells away from the source at (11 Δs, 11 Δs, 19 Δs). Fig. 12 shows the performance of C-COM4 (2, 8) and C-COM4 (8, 8). Finally, we note that the C-COM4 (8, W) yields a higher accuracy solution, however, its memory burden is substantial and, thus, it is recommended that it be reserved for applications with more stringent accuracy requirements.

V. Error Analysis

In this section, we will focus on the error canceling mechanism of the C-COM implementation. For illustration and without any loss of generality, we will only give analysis based on reflections from side boundaries.

When the averaging interface is positioned at a distance from the terminal boundary that exceeds the width of the

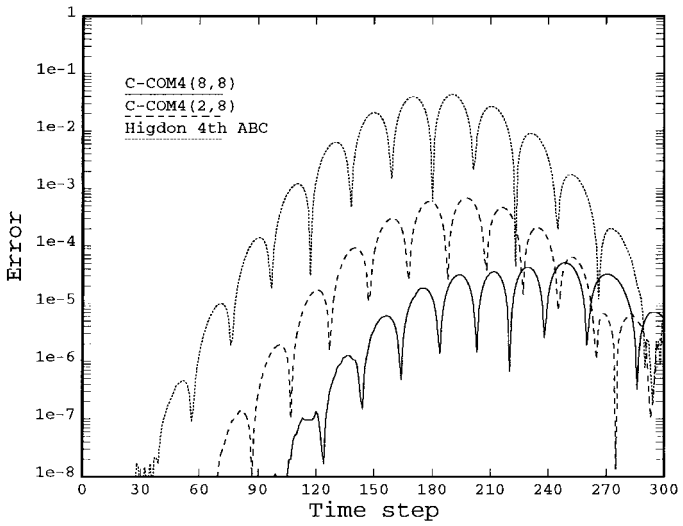

Fig. 12. Results for the problem of the Hertzian dipole radiating in free-space.

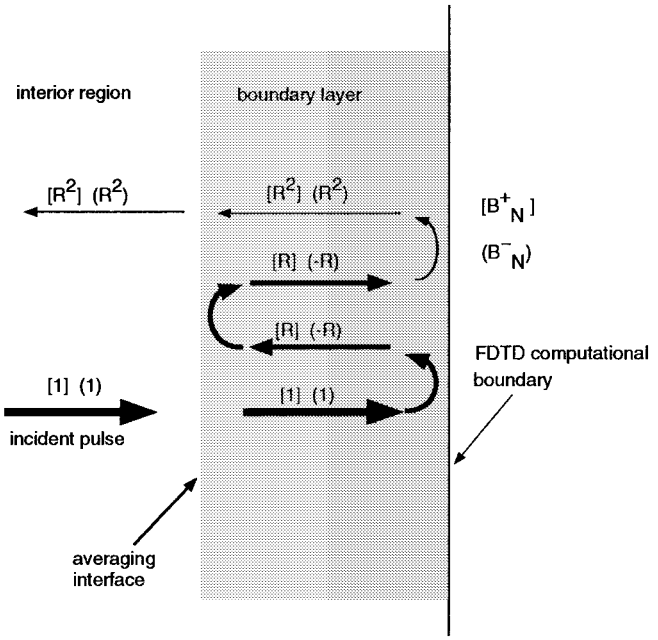

Fig. 13. Illustration showing the cancellation mechanism of the C-COM method.

stencil needed to discretize the ABC, a virtual or nonphysical discontinuity is effectively created at this interface. When the fields (corresponding to each of the two field sets in the boundary layer) are reflected off the boundary, each will have an error which is opposite in phase but equal in magnitude to the other. Averaging these two solutions leaves the field in the interior region with no error. In other words, the nonphysical boundary results in a reflection back into the boundary layer of the first reflection. The complete reflection of the first-order error at the interface must take place in order to satisfy the continuity of the field at the interface. An illustration of these reflections is shown in Fig. 13 where the reflection that occurs when B_N^- is enforced is shown in brackets while the reflections due to B_N^+ are shown in parentheses.

The first reflection goes back to the terminal boundary and is partially reflected, giving rise to a second reflected wave. The second reflections due to each of the two complementary operators have equal magnitudes and are *in phase* unlike the first reflections. Consequently, when the second reflections are averaged at the interface, no cancellation takes place and these reflections penetrate into the interior region.

Therefore, the net effect of implementing the complementary operators in a concurrent fashion is to double the order of the reflection coefficient of each of the complementary operators in (1) or (2). More specifically, if the complementary ABC's give a reflection coefficient of magnitude $|R|$, then the C-COM implementation results in a reflection coefficient of R^2, in addition to a propagation delay equivalent to twice the width of the boundary layer.

A quantitative study of the performance of the C-COM is performed by analyzing the reflection of a plane wave from the terminal side boundary. We set up a numerical experiment in which we simulate the reflection of a plane wave with varying angle of incidence. We consider a 2-D space of size 210 $\Delta s\times$ 1400 Δs. A perfectly conducting screen is positioned across the entire computational domain at $x = 200\Delta s$. The cell size and the time step are chosen as before for the 2-D space experiments.

An incident field is propagated from the left-hand side of the domain starting at the terminal boundary. The time waveform of the incident plane wave is given by

$$f(t) = (1.0 - e^{-(\tau/T_w)^2}) \sin(c\tau 2\pi/\lambda) \tag{8}$$

where $T_w = 20\Delta t$, $\tau = t - x/c$, and $\lambda = 36\Delta s$. This time waveform is a sinusoidal signal with a smooth initial transition to obtain faster convergence.

The function $f(t)$ satisfies Maxwell's equations and it represents a plane wave incident normally at the screen coming from the left-hand side (negative x direction). To simulate the effect of a plane wave with an angle of incidence different from normal incidence, we adjust the angle ϕ in Higdon's ABC operators [see (1) and (2)]. (For this problem, we use a scattered field formulation where the incident wave interacts only with the screen.) Next, we apply C-COM2 (2, 20) and observe the maximum magnitude of the reflected pulse at an observation point located at (30, 700). This particular location of the observation point ensures that the reflections from the horizontal side boundaries do not interfere with the solution which is observed over the first 1500 time steps. The C-COM2 instead of the C-COM4 was chosen to allow for clear quantization of the reflection. Had we applied C-COM4, the reflections would be very difficult to isolate considering the artifacts of the simulation (for instance, at $\phi = 30°$, R(C-COM4) $= 1.37 \times 10^{-7}$.

Fig. 14 shows the reflection coefficient calculated using Higdon's first-order ABC and the C-COM2 solution as obtained numerically and as predicted (calculated) from theory. An excellent match is observed between theory and experiment since $|R$(C-COM2)$| = |R$ (Higdon's first-order ABC)$|^2$.

An additional factor that further reduces the reflection coefficient in practical applications and is more difficult to quantify is attributed to the delay that the reflected waves experience

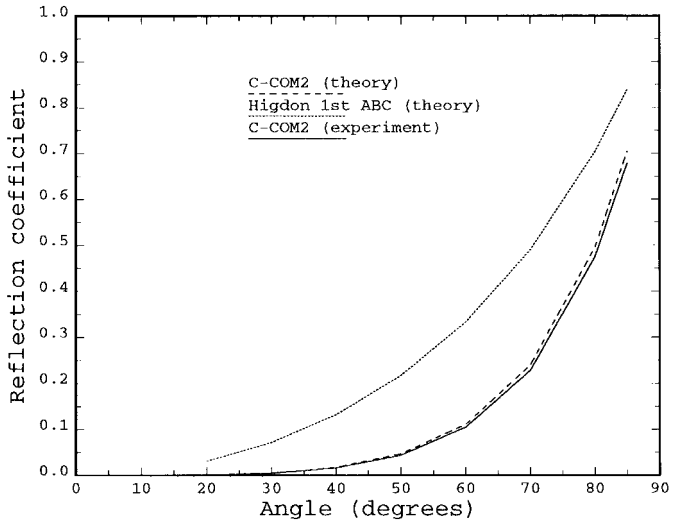

Fig. 14. Reflection coefficients for Higdon's first-order ABC and C-COM2.

during their multiple reflections within the boundary layer. Such delay causes the second reflected wave that penetrates into the interior region to be diminished in magnitude. This delay can be interpreted as a virtual enlargement of the computational space. This is a significant advantage when the fields contain sufficient energy in the evanescent spectrum.

This analysis also explains why the averaging interface cannot be positioned within the stencil needed for B_N^+ or B_N^- (see Fig. 3). The stencil defines the domain of application of Higdon ABC, which is constructed based on the one-way wave equation in a uniform and homogeneous space. The averaging of the fields at the interface creates a discontinuity of the reflected fields, which is equivalent to positioning a source at the interface. Such source cannot be allowed within the stencil of the ABC. Numerical experiments have shown that the solution grows without bound within several time steps after the field reaches the terminal boundary.

VI. Summary

A novel implementation of the complementary operators method is presented. This new implementation is based on the application of complementary operators at a distance from the terminal boundaries such that first-order reflections are annihilated before they enter the computational domain. The method is very simple to implement since it is based on the one-way wave equations such as Higdon's boundary operators.

The major accomplishment of the C-COM method is the implementation of complementary operators without the need for two independent simulations as was originally conceived in the COM method. Furthermore, the C-COM theory allows for the annihilation of corner reflections with reasonable efficiency in the 2-D space. In the 3-D space, the annihilation of corner reflections levies a heavy memory burden and it is, therefore, reserved for applications in which substantial computational overhead justifies the desired accuracy.

The performance of the C-COM has been proven highly effective yielding unprecedented levels of suppression of spurious terminal boundary reflections. The strength of the C-COM method was especially demonstrated for waves incident at terminal boundaries at near grazing incidence. This makes the C-COM well-suited for FDTD studies of atmospheric propagation. Finally, we note that unlike the COM method, the C-COM extends the scope and applicability of the complementary operators theory to the efficient treatment of nonlinear media.

Acknowledgment

The author would like to thank J. Schneider for many helpful discussions and for reviewing the manuscript.

References

[1] O. M. Ramahi, "Application of the complementary operator method to the finite-difference time-domain solution of the three-dimensional radiation problem," *Microwave Opt. Technol. Lett.*, vol. 9, no. 3, pp. 147–149, June 1995.

[2] ———, "Complementary operators: A method to annihilate artificial reflections arising from the truncation of the computational domain in the solution of partial differential equations," *IEEE Trans. Antennas Propagat.*, vol. 43, pp. 697–704, July 1995.

[3] ———, "Complementary boundary operators for wave propagation problems," *J. Computat. Phys.*, vol. 133, pp. 113–128, 1997.

[4] O. M. Ramahi and J. Schneider, "Comparative study of the PML and COM," *IEEE Microwave Guided Wave Lett.*, vol. 8, pp. 55–57, Feb. 1998.

[5] O. M. Ramahi, "Concurrent implementation of the complementary operators method in 2-D space," *IEEE Microwave Guided Wave Lett.*, vol. 7, pp. 165–167, June 1997.

[6] J.-P. Berenger, "A perfectly matched layer for the absorption of electromagnetic waves," *J. Computat. Phys.*, vol. 114, pp. 185–200, 1994.

Omar M. Ramahi (M'97) received the B.S. degree in electrical engineering and mathematics (highest honors) from Oregon State University, Corvallis, in 1984, and the M.S. and Ph.D. degrees in electrical engineering from the University of Illinois at Urbana-Champaign, in 1986 and 1990, respectively.

From 1990 to 1993, he was a Postdoctoral Research Fellow at the University of Illinois at Urbana-Champaign. Since 1993 he has been with Digital Equipment Corporation, Maynard, MA. He is the coauthor of *EMI/EMC Computational Modeling Handbook* (Norwell, MA: Kluwer, 1998). He has published more than 70 conference and journal papers. His interests include applied and computational physics, radiation phenomenon, antennas, microwave and high-speed digital circuits packaging, and medical applications of electromagnetics.

Dr. Ramahi is a member of the Electromagnetics Academy.